Crystallization-induced emission enhancement of alkyl chain-dependent pyrene-based luminogens: Visual detection of nitro-explosives

Ze-Dong Yu,[a] Jing-Yi Cao,[a] Hua-Long Li,[a] Guang Yang,[a] Wen-Xuan Zhao,[a] Chuan-Zeng Wang*[a,b], Shu-Hai Chen,*[a] Mark, R.J. Elsegood,[c] Carl Redshaw,[d] and Takehiko Yamato,*[b]

[a] School of Chemistry and Chemical Engineering, Shandong University of Technology, Zibo 255049, P. R. China

[b] Department of Applied Chemistry, Faculty of Science and Engineering, Saga University Honjo-machi 1, Saga 840-8502 Japan

[c] Chemistry Department, Loughborough University, Loughborough, LE11 3TU, UK

[d] Department of Chemistry, The University of Hull, Cottingham Road, Hull, Yorkshire HU6 7RX, UK

Abstract:

In view of the widespread applications and urgent need for efficient blue emitting materials, the synthesis of such materials has seen renewed interest. In the present work, three alkyl chain-dependent blue emitting pyrene-based luminogens were synthesized and characterized. The experimental results show that these luminogens exhibited high photoluminescence efficiency both in solution (> 86%) and in the solid state (35%). Interestingly, **TAPy**, as a photoelectric functional material, was endowed with higher quantum yield (72%) and competitiveness due to a remarkable crystallization-induced emission enhancement (CIEE) property. More importantly, **TAPy** exhibits high sensitivity and selectivity for ***o*-NA** with low limit of detection (9.99×10^{-8} M), which is mainly due to the distinctive odd-even effects of the terminal alkyl chain. The results demonstrate that this type of luminogen can potentially be utilized for practical applications in the field of contaminant or explosive detection as a sensitive and portable fluorimeter.

Keywords: Crystallization-induced emission enhancement; Pyrene chemistry; Nitro-explosives; Sensing properties

Introduction

The proven and effective sensing technologies available for the detection of trace amounts of dangerous nitro-explosives have aroused great interest recently due to their feasible applications for land security and environmental pollution [1,2]. These techniques utilize the likes of Raman spectroscopy [3] and ion mobility spectroscopy [4], but these are susceptible to interference from fluorescent or strongly absorbing materials and require rigorous pre-treatment of samples. Moreover, expensive and cumbersome procedures are often involved, and these limit the real-time use of such techniques. Among the various types of detection methods, sensors have gradually gained more importance due to their properties of portability, customizable, multimodal capability, cost-effectiveness, and ease of use [5-9]. To date, the use of fluorescent materials has great potential, particularly for explosives detection, as they involve interactions between the explosives and the chemoreceptor, which results in changes of absorption/emission properties. Indeed, systems involving metal-conjugated frames [10,11], organic micro molecules [12-14], aggregation-induced emission luminogens (AIEgens) and polymeric systems [15-18] have become attractive detection methods for nitroaromatic compounds (NACs). Recently, interest has been directed towards the design of “turn-off” fluorescent probes because of their great advantages in visual and rapid detection. However, the preparation of efficient fluorescent probes with high quantum yields and reversibility is challenging due to their large Stoke’s shift and aggregation-caused quenching (ACQ) character [9,19,20].

Pyrene, as a luminescent material, possesses both disadvantages and advantages [21,22]. For instance, the common ACQ phenomenon can occurs with low fluorescence quantum yield due to the formation of π-aggregate/excimer in the solid state. Thus, many efforts have been made to address this issue, and the most effective strategies are to design functional pyrene-based materials with AIE, crystallization-induced emission

(CIE), clusterization-triggered emission (CTE), aggregation-induced anti-Kasha transition, or aggregation-induced delayed fluorescence (AIDF) properties [23-27]. The resulting modified materials can be better applied to practical applications.

In the development of pyrene-based full-color luminescent materials, the design of blue emitting materials is challenging due to their large energy gaps [28]. Given this, accessing pyrene-based blue emitting materials with high color purity and luminescence quantum yield remains one of the main focuses in the field of optoelectronic materials. Herein, a series of alkyl chain-dependent pyrene-based luminogens with blue emission were synthesized in good yields (Scheme 1). Interestingly, all luminogens exhibited excellent fluorescence quantum yields of over 86% in dilute solution, and compound **TAPy** displayed a crystallization-induced emission enhancement (CIEE) effect, which resulted in an increased value of Φ_{FL} up to 72%. In addition, selective visual detection of nitro-explosives with obvious quenching efficiency was possible by employing the above luminogens.

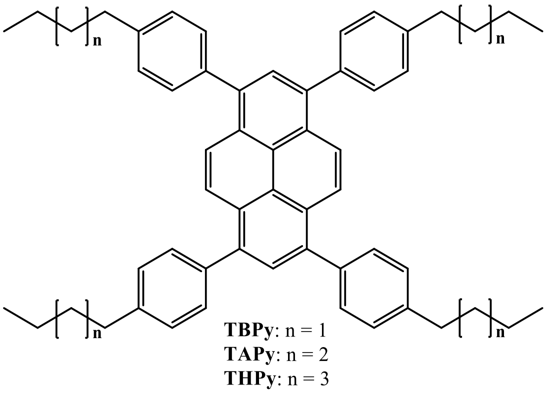

Scheme 1 Chemical structures of **TBPy**, **TAPy** and **THPy**.

Results and discussion

Synthesis and characterization

Based on both solubility and performance considerations, three alkyl chain-dependent pyrene-based luminogens were designed and synthesized from tetrabromopyrene [29] as the starting compound *via* a Suzuki coupling reaction; all target compounds were obtained in good yields (> 87%). Subsequently, these structures were characterized in detailed by ^{1}H- and ^{13}C-NMR spectroscopy (Fig. S1–6, ESI‡), high resolution mass spectrometry, as well as by single-crystal X-ray diffraction for **TAPy** (Table S1, ESI‡). The crystallographic results allowed us to further evaluate the influence of these *para*-alkyl chains on the phenyl groups in terms of their packing arrangement and photophysical properties. Initially, the torsion angles between the pyrene core and the phenyl moieties was measured, and compared to the reference compound 1, 3, 5, 9-tetraphenylpyrene (**TPPy**) [29]. It was found that **TAPy** displayed larger torsion angles (53.09°, 53.61°, 62.50°, 63.41°) due to the alkyl moieties appended to the phenyl groups (see Fig. 1A and B), which may provide important evidence for interpreting the structure–property relationships and emission mechanisms in the aggregated state [30].

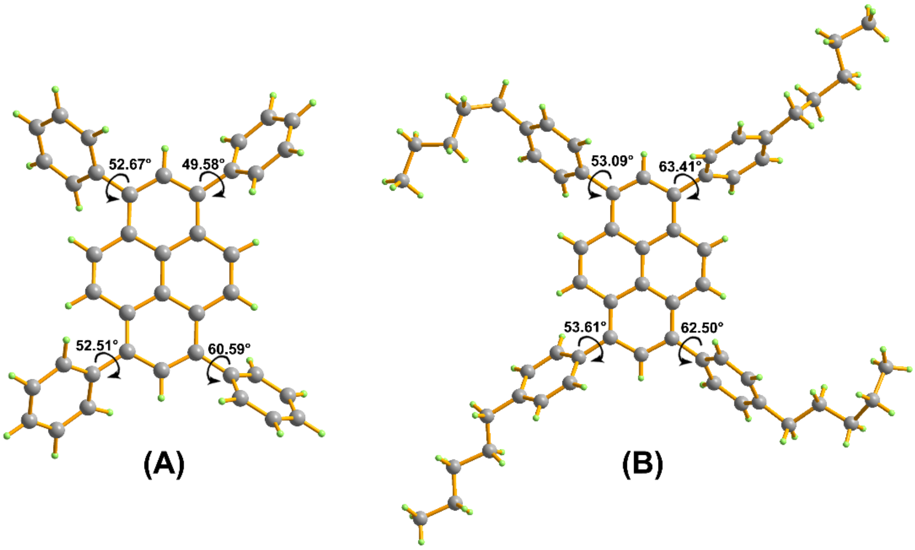

Fig. 1 Crystal structures of **TPPy** and **TAPy**: showing the different torsion angles between the pyrene core and the phenyl moieties.

Further investigation on the molecular packing was performed. Fig. 2A and B show details of the stacking and interactions of the **TAPy** molecules, and a compact layered arrangement formed with the assistance of hydrogen bonding was observed. Generally speaking, classical or unusual C−H···C hydrogen bonds, with 2.6−3.3 Å in length, are usually weak but play a crucial role in structural stability [31]. Herein, a large number of hydrogen bonds with short-distance contacts (2.421−2.867 Å, Fig. 2C) are present and result in a stable molecular assembly, which inevitably leads to inhibition of molecular motion in the crystalline state. Weakened non-radiative pathways then contribute to radiative transition, so high efficiency luminescence for **TPPy** may present in the crystalline state [35,36]. Thus, crystallization-induced emission (CIE) or crystallization-induced emission enhancement (CIEE) may be a desirable property in this system. In that case, alkyl chain-dependent pyrene-based luminogens will be endowed with higher competitiveness in materials science [26].

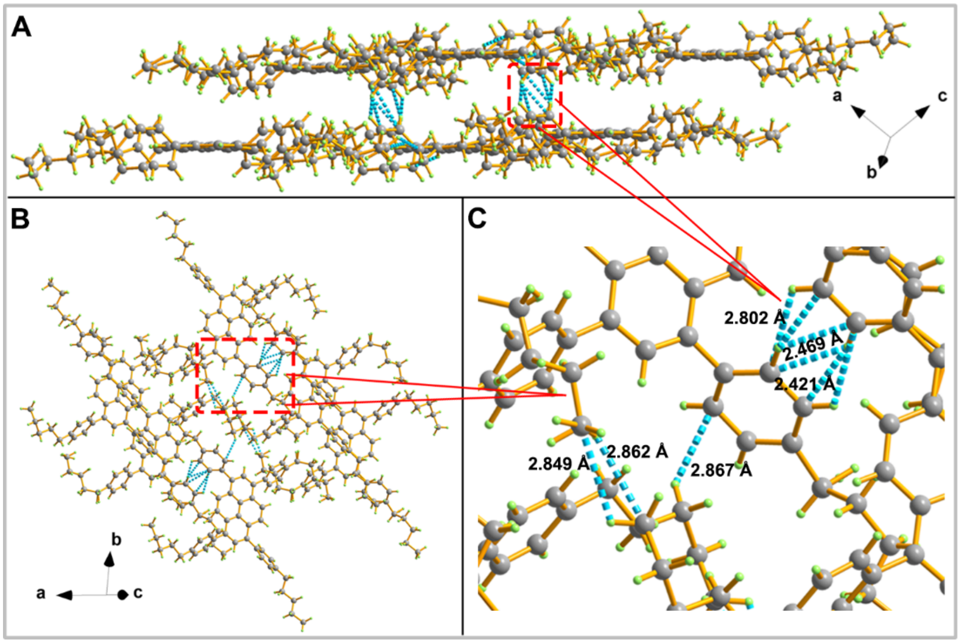

Fig. 2 Packing motif and detailed intermolecular interactions in the crystal structure of **TAPy**.

Photophysical properties

Table 1. The photophysical properties of **TBPy**, **TAPy** and **THPy**.

Compounds	λ_{abs}(nm) sol[a]	λ_{em}(nm) sol[b]/solid/crystal	Φ_{FL}[c] (%) sol[a]/solid/crystal	HOMO (eV)	LUMO (eV)	E_g (eV)
TBPy	300, 383	436 / 472 / nd[d]	86 / 35 / nd	−4.88	−1.58	3.30
TAPy	299, 381	436 / 492 / 470	87 / 46 / 72	−4.88	−1.58	3.30
THPy	300, 386	438 / 477 / nd	88 / 36 / nd	−4.89	−1.56	3.33

[a] ~×10^{-5} M in CH_2Cl_2, λ_{abs} is the absorption band appearing at the longest wavelength.
[b] ~×10^{-7} M in CH_2Cl_2, λ_{em} is the fluorescence band appearing at the shortest wavelength.
[c] Absolute quantum yield (± 0.01–0.03).
[d] nd: not detect.

Following the structural characterization, the photophysical properties of **TBPy**, **TAPy** and **THPy** were also studied in dilute solutions and in the solid state; relevant parameters are listed in Table 1. Firstly, all three luminogens exhibited highly similar absorption bands and emission spectra in dilute organic solutions. As shown in Fig. 3A, two sets of clear and smooth absorption bands with peaks in the 381−386 nm range and around 300 nm. The high energy absorptions centered at 299 or 300 nm are mainly ascribed to the π-π* transition of the pyrene core and alkyl-substituted phenyl groups. Comparatively speaking, the low energy bands exhibited slight differences between the three luminogens (383 nm for **TBPy**, 381 nm for **TAPy,** and 386 nm for **THPy**), which can be ascribed to the intramolecular charge transfer (ICT) transition from several alkyl chains to the extended π system.

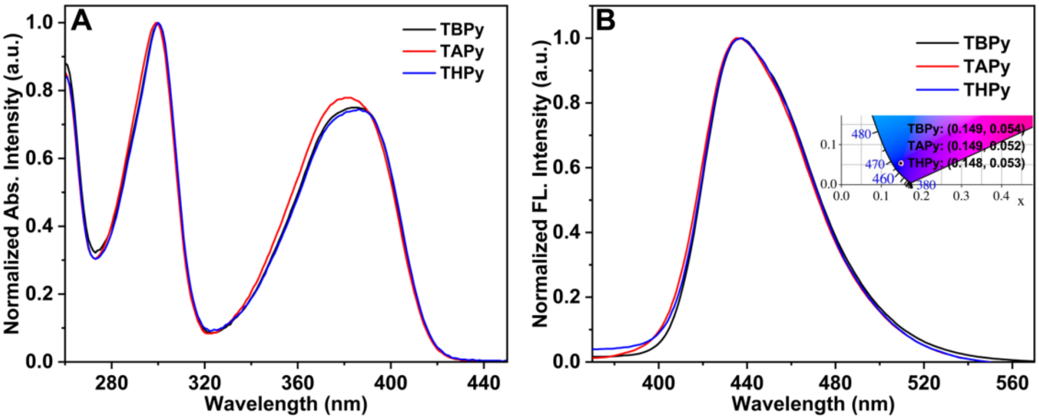

Fig. 3 UV-Vis absorption (A) emission spectra (B) for luminogens **TBPy**, **TAPy** and **THPy** in DCM solution (Insets: CIE 1931 chromaticity diagram for **TBPy**, **TAPy** and **THPy**).

As can be seen from Fig. 3B (and the inset), a subtler difference was observed for their emission spectra, with the monomeric emission playing a dominant role in dilute organic solution, and the peripheral substituent groups only exerting a slight influence on their emitting materials. The series of deep-blue pyrene-based luminogens with high quantum yields (> 86%) in DCM solution exhibited a superior performance as photoelectric materials, which provide a design strategy for the preparation of deep-blue luminescent materials. Subsequently, the solvatochromic effects were studied in order to gain some insight into the absorption and emission behavior. As shown in Figures S7-S12, similar red-shifts at short-wavelength band and long-wavelength band were observed with 2-7 nm range for their absorption spectra in different solvents with varying polarity (cyclohexane; 1,4-dioxane; tetrahydrofuran: THF; dichloromethane: DCM; and dimethyl formamide: DMF). On the other hand, the emission spectra of all three luminogens exhibited the same red-shift (5 nm) on moving from the nonpolar solvent cyclohexane to the polar solvent DMF. Such results are consistent with an insignificant solvatochromic effect, which indicates that the intramolecular charge transfer behavior is minimal in this symmetrical system. This also indicated that there is no dependency between the intramolecular charge transfer transitions and the length of the *n*-alkyl chains [34,35]. In order to confirm this conclusion, density functional theory (DFT) calculations were performed to obtain a deeper insight into the microcosmic effect based on energies of the highest occupied molecular orbitals (HOMOs) and the lowest unoccupied molecular orbitals (LUMOs) at the B3LYP-D3/6-31G(d) level [36,37]. As expected, the contours of the HOMOs and LUMOs of **TBPy**, **TAPy** and **THPy** present similar distributions, and which are mainly dispersed over the π-system involving the pyrene core and phenyl rings (see Fig. 4). Moreover, although the terminal alkyls are different, the band gaps (ΔE_g) of the HOMO-LUMO displayed subtle differences or were even identical, and these theoretical calculations are strongly consistent with the photophysical properties observed in dilute solution. Meanwhile, this result also confirmed the conclusion mentioned above that the ICT behavior is not obvious in this system.

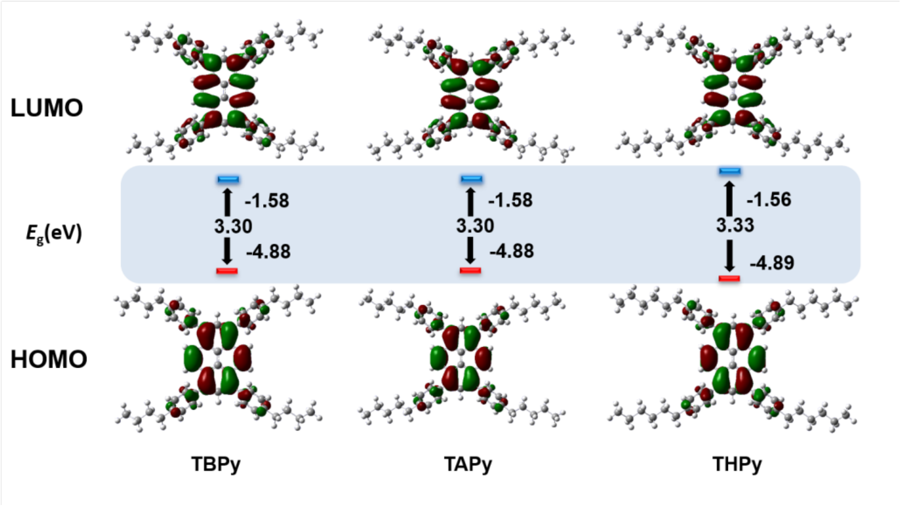

Fig. 4 Frontier-molecular-orbital distributions and energy level diagrams for **TBPy**, **TAPy** and **THPy** by DFT calculations.

Investigation of the aggregate states brought more interesting results, compared to the highly similar optical physical properties noted in solution. The *para* alkyl substituents on the terminal phenyls have an obvious influence on the emission properties both in the solid state and in crystalline state. As shown in Fig. 5, the maximum emission wavelengths are 472 nm for **TBPy**, 492 nm for **TAPy**, and 477 nm for **THPy** in the solid state, respectively. Significantly, **TAPy** reveals a distinct red-shift relative to the other two compounds, which may be attributed to the influence of the respective influence of their alkyl chains on the terminal phenyl moieties [38]. Meanwhile, **TAPy** with odd-numbered alkyl chains exhibited higher fluorescence quantum yields ($\Phi_{\mathrm{FL}} = 46\%$) than **TBPy** ($\Phi_{\mathrm{FL}} = 35\%$) and **THPy** ($\Phi_{\mathrm{FL}} = 36\%$) with even-numbered alkyl chains, and dimeric/excimeric emission may be dominant for these three luminogens. Generally, red-shifted and quenched emission are regular phenomenon from dilute solutions to the aggregated states due to the enhanced π–π interactions [39]. However, **TAPy** with a higher absolute Φ_{FL} than the other two compounds have proven once again the parity effect existing in this system, which may be attributed to the formation of discrete π–π dimer stacking in the solid state [40]. Overall, as solid, the materials for this work are promising candidates in the field of photoelectric materials with reasonable Φ_{FL} more than 35%. What's more, this strategy demonstrated its greater advantage and efficiency when we studied the photophysical properties of **TAPy** in the crystalline state. The obvious blue-shift (22 nm) with enhanced emission (the value of Φ_{FL} up to 72%) presents an effective strategy to achieve novel pyrene-based luminescent materials. In detail, the phase transition from dimer to monomer should be the mainly trigger, as indicated by Fig. 2, possible π–π dimer stacking was not observed, to be replaced by a compact layered arrangement, and the pyrene cores are staggered in relation to each other with abundant C–H···C hydrogen bonds interactions in the same layer and different layers [41]. Thus, the typical CIEE phenomenon with a near doubling in Φ_{FL} (up to 72%) was afforded by restricting the intramolecular motions and blocking the non-radiative channels in the crystalline state [42].

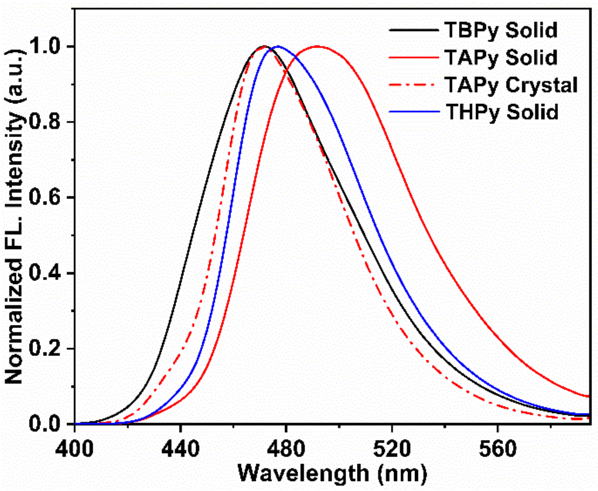

Fig. 5 Emission spectra for luminogens **TBPy**, **TAPy** and **THPy** in the solid state and for **TAPy** in the crystalline state.

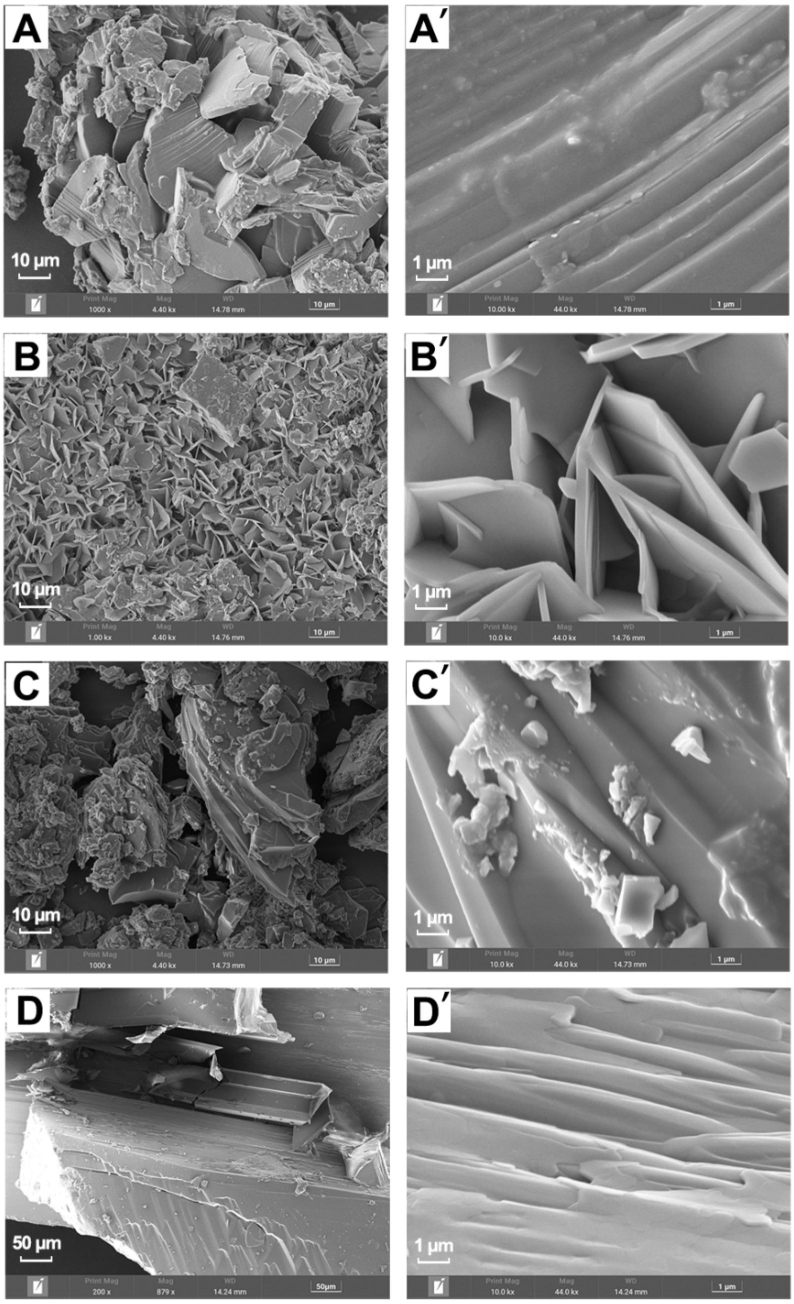

Fig. 6 SEM microphotographs of powder **TBPy** (A and A'), **TAPy** (B and B'), **THPy** (C and C') and crystal **TAPy** (D and D') with different magnification, respectively.

All samples including powders for **TBPy**, **TAPy**, **THPy** and crystals for **TAPy** were further analyzed for their morphology by scanning electron microscopy (SEM). As can be seen from Fig. 6A and C, the **TBPy** (A and A') and **THPy** (C and C') are characterized by compact lamellar sheets with lengths of up to several tens of micrometers and a thickness above a few hundred nanometers. These results indicate the possibility of the formation of excimer emission by face-to-face interactions between the planar pyrene moieties based on strong π···π interactions, which is also consistent with the low quantum yield in the experimental results. In stark contrast, the powder of **TBPy** (Fig. 6B and B') is a homogeneous rhomboid sheet approx. 0.1 micrometers thick and ten micrometers long, which is further verified the hypothesis that **TAPy** displayed a higher quantum yield than **TBPy** and **THPy**, which is ascribed to the distinct packing arrangement in the aggregate state [43,44]. Interestingly, the morphological structure of **TAPy** was investigated by scanning from different perspectives as shown in Fig. 6 and Fig. S13. Both sets of SEM results indicate that the molecule packing is compact but different from powdered **TBPy** and **THPy**. In this case, the adjacent pyrene cores are completely slipped, which combined with abundant hydrogen bonds, leads to intense emission with high Φ_{FL} value 72%, and the CIEE result is comparable to many reported AIE materials [25, 45].

Detection of nitroaniline

Efficient alkyl chain-dependent blue pyrene-based luminogens with large energy band gaps (> 3.30 eV) are expected to be used in chemosensors based on Förster resonance energy transfer (FRET) [46-48]. Indeed, more overlap area between the absorption band of the analyte and the emission band of the luminogens is more likely to give rise to fluorescence quenching. Thus, taking into account the excellent emission properties of these compounds (Fig. 7A), especially for **TAPy**, a large overlap was observed with a green shadow. We investigated the detection results by testing multiple sets of standard DCM solutions containing different nitroaniline (**NA**) concentrations which varied from 0.2 to 2 mmol L^{-1}. Taking **TAPy** and ***o*-NA** as an example, as shown in Fig. 7B, a significant and persistent quenching was observed along with an increase of ***o*-NA** concentration. This luminescence quenching efficiency is up to 92.1%, which rivals or is even better than that for reported pyrene-based sensors used for nitro-explosives detection [48,49]. In contrast, the other two nitroanilines exhibited relatively weak quenching for **TAPy** under the same optimized conditions with a low quenching efficiency of about 70.4% for ***m*-NA** and 74.0% for ***p*-NA**. Moreover, **TBPy** and **THPy** also displayed similar quenching efficiency, and the values for **TBPy** were found to be 90.8% for ***o*-NA**, 71.8% for ***m*-NA** and 74.7% for ***p*-NA**, and the values for **THPy** were found to be 89.9% for ***o*-NA**, 71.0% for ***m*-NA** and 62.8% for ***p*-NA**. These compounds exhibited selectivity for nitro-explosives, which can be better represented by the Stern–Volmer (SV) equation: $(I_0/I) = 1 + K_{sv}\,[Q]$, where is the quenching constant (M^{-1}), [Q] is the molar concentration of nitro explosives (*m*M), I_0 and I are fluorescence intensities before and after the addition of the nitro explosives, respectively. As shown in Fig.7D, for **TAPy**, the quenching constants K_{sv}, 5370 M^{-1} for ***o*-NA**, 1240 M^{-1} for ***m*-NA** and ***p*-NA**, show the selectivity the detection. Subsequently, the standard deviation and limit of detection (LOD) were calculated (see Fig. S14 and detailed procedure in the supporting information). The LOD was found to be 9.99×10^{-8} M for the **TAPy/*o*-NA** system based on the equation: LOD= $3\sigma/K$, and all three luminogens show high sensitivity and selectivity to nitro-explosives (Figures S15-S18).

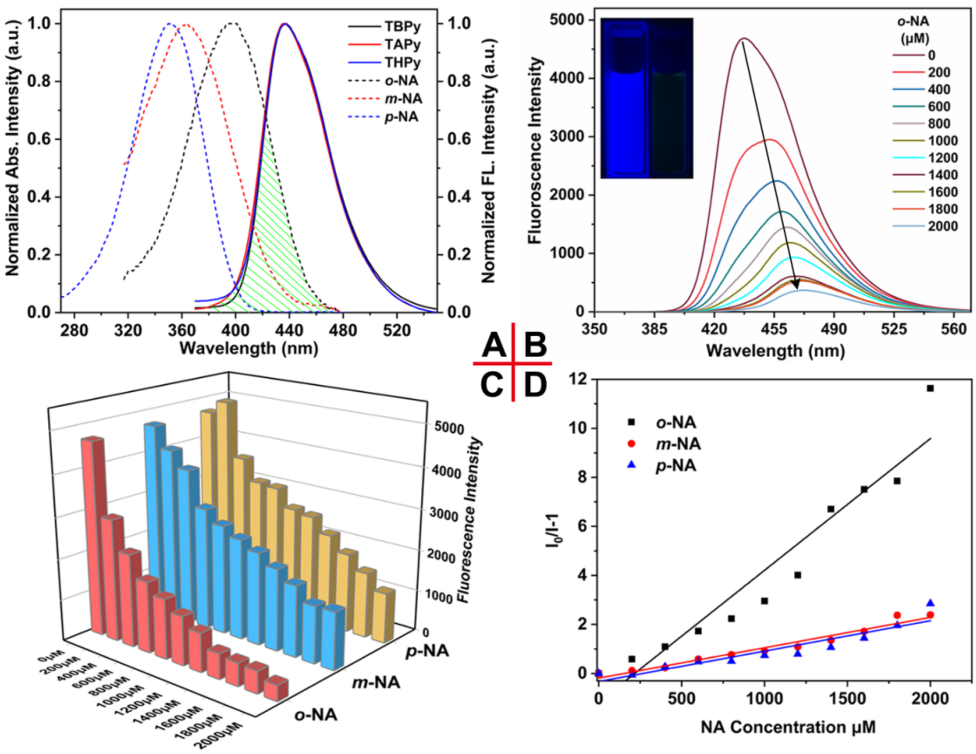

Fig. 7 Normalized absorption spectra of **NA** and fluorescence spectra of luminogens in DCM (A), fluorescence quenching of **TAPy** with incremental addition of ***o*-NA** and inset photographs show the visible change in the fluorescence under UV light before and after addition of ***o*-NA** (B), the histogram of fluorescence quenching of **TAPy** with **NA** (C), corresponding Sterne-Volmer plots for

fluorescence quenching of **TAPy** in the presence of **NA** as quencher in DCM (D).

In order to verify the highly selective and sensitive sensing behavior of **TAPy** towards nitro-explosives, further experiments were performed by evaluating the performance as a portable solid-state fluorescence sensor for nitro-explosives. Qualitative filter paper coated with **TAPy** was selected to carry out the qualitative detection of **NA** under 365 nm UV irradiation. It was even better than expected, and the identification of these three nitroaniline is more significant than in solution. As shown in Fig. 8, compared to the reference strips (blank groups), the test strips were contaminated by **NA** presenting distinct quenching efficiency and speed. Specifically, a more sensitive and efficient result was observed for the ***o*-NA** system, which is also consistent with previous results in solution. In stark contrast, especially for ***p*-NA**, a slight quenching was observed even after a longer time period. Thus, an efficient and portable fluorimeter is expected to be used to detect nitro-explosives, particularly nitroaniline.

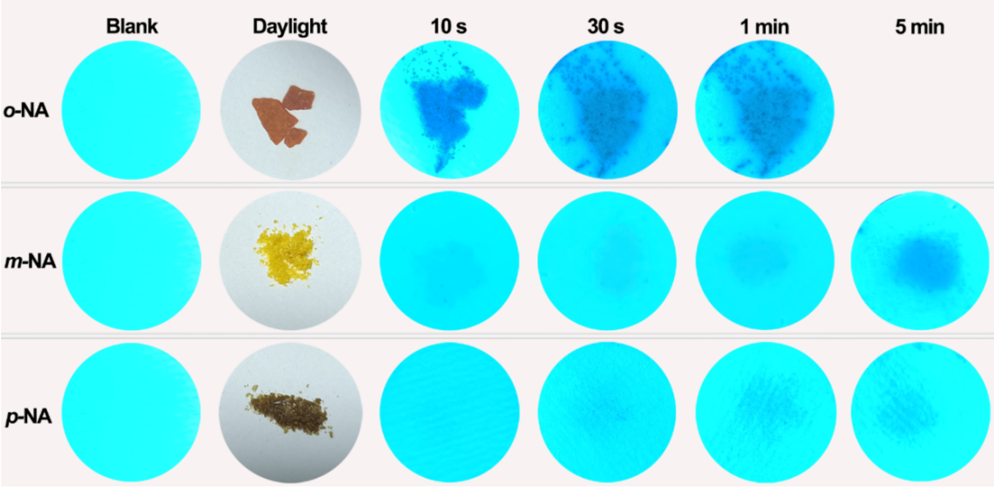

Fig. 8 Test strips of **TAPy** and its response to **NA** powders under UV irradiation under different time conditions.

Conclusions

In summary, a series of alkyl chain-dependent pyrene-based luminogens with high quantum yields are presented. Distinct photophysical properties, especially in the aggregate states, were observed due to the influence of the parity effect of their alkyl chains on the terminal phenyl moieties, including CIEE phenomenon, photoluminescence efficiency and molecular alignment, which provide a novel strategy to construct pyrene-based CIE or deep blue-emitting luminogens. Based on these differences, a visual selective detection of nitro-explosives for potential real-world application was developed with a very desirable limit of detection. Such a system can provide an efficient approach to reduce the illegal transportation of nitro-explosives and terrorist attacks.

Experimental Section

Materials and methods

All chemicals were purchased from commercial suppliers (Leyan reagent, Aladdin) and were used without further purification. All the reactions were carried out using a round bottom flask under a nitrogen atmosphere in anhydrous solvents. ^{1}H and ^{13}C NMR spectra were obtained in $CDCl_3$ on a WJGS-037 Bruker AVANCE III 400 MHz NMR spectrometer, using tetramethyl silane (TMS) as the internal standard. Mass spectrometry data were recorded on an Agilent 1290 Infinity. UV-vis absorbance and photoluminescence (PL) spectra were recorded on a Shimadzu UV-3600 and a Fluorescence spectrophotometer F-380A, respectively. Photoluminescence quantum efficiencies (PLQYs) were measured using Quantaurus-QY C11347-11. All the P-XRD parameter was presented using D8 ADVANCE.

Synthesis

1, 3, 6, 8-Tetrabromopyrene **1** was readily obtained by the exhaustive bromination of pyrene by following the previously reported procedure [29]. Target compounds were further synthesized following Scheme S1.

Synthesis of 1, 3, 6, 8-tetrakis (Butylphenyl) pyrene (TBPy)

Into a 250 mL round bottom flask equipped with a magnetic stirring bar was placed 1, 3, 6, 8-tetrabromopyrene (0.65 g, 1.25 mmol), 4-(butylphenyl) boronic acid (1.70 g, 7.50 mmol), $Pd(PPh_3)_4$ (0.044 mg, 10%M) and aqueous 2.0 M Cs_2CO_3 (80 mL) containing nitrogen saturated toluene (50 mL) and absolute ethyl alcohol (20 mL). The reaction mixture was stirred at 110 °C for 48 h. After it was cooled to room temperature, the mixture was diluted with water (60 mL) and extracted with dichloromethane (80 mL × 2). The organic layer was washed with brine solution, dried with anhydrous $MgSO_4$ and concentrated under reduced pressure. The crude product was purified by column chromatography using hexane/dichloromethane (9:1, v/v) as an eluent to give compound **TBPy** as a dark yellow powder (0.87 g, 94.8%); M.P. 207-209 °C; ^1H NMR (400 MHz, $CDCl_3$): δ_H =8.18 (s, 4H, pyrene-*H*), 8.00 (s, 2H, pyrene-*H*), 7.58 (d, *J* = 7.4 Hz, 8H, Ph-*H*), 7.34 (d, *J* = 7.4 Hz, 8H, Ph-*H*), 2.74 (d, *J* = 7.6 Hz, 8H, Alkyl-*H*), 1.73 – 1.67 (m, 8H, Alkyl-*H*), 1.44 (m, *J* = 14.7 Hz, 7.3 Hz, 8H, Alkyl-*H*), 0.98 (t, *J* = 7.3 Hz, 12H, Me); ^{13}C NMR (100 MHz, $CDCl_3$): δ_C = 141.94, 138.45, 137.15, 130.53, 128.38, 128.06, 126.08, 125.23, 35.46, 35.29, 33.71, 22.45, 14.01; FAB-MS: m/z calcd for $C_{56}H_{58}$ 731.4617 [M^+]; found 731.4589[M^+].

A similar procedure using 4-(amylphenyl) boronic acid, 4-(hexylphenyl) boronic acid was followed for the synthesis of **TAPy** and **THPy**.

Synthesis of 1, 3, 6, 8-tetrakis (Amylphenyl) pyrene (TAPy)

Compound **TAPy** was obtained as a pure yellow solid (0.93 g, 94.0%); M.P. 121-125 °C; ^1H NMR (400 MHz, $CDCl_3$): δ_H = 8.19 (s, 4H, pyrene-*H*), 8.00 (s, 2H, pyrene-*H*), 7.58 (d, *J* = 7.4 Hz, 8H, Ph-*H*), 7.34 (d, *J* = 7.4 Hz, 8H, Ph-*H*), 2.72 (t, *J* = 7.5 Hz, 8H, Alkyl-*H*), 1.72 (s, 8H, Alkyl-*H*), 1.40 (s, 16H, Alkyl-*H*), 0.93 (s, 12H, Me); ^{13}C NMR (100 MHz, $CDCl_3$): δ_C =141.98, 138.44, 137.15, 130.53, 129.58, 128.36, 128.05, 126.07, 125.23, 35.74, 31.60, 31.24, 22.60, 14.07; FAB-MS: m/z calcd for $C_{60}H_{66}$ 787.5243 [M^+]; found 787.5219[M^+].

Synthesis of 1, 3, 6, 8-tetrakis (Hexylphenyl) pyrene (THPy)

Compound **THPy** was obtained as a pure yellow solid (0.55 g, 87.0%); M.P. 93-95 °C; ^1H NMR (400 MHz, $CDCl_3$): δ_H = 8.19 (s, 4H, pyrene-*H*), 8.00 (s, 2H, pyrene-*H*), 7.57 (d, *J* = 7.4 Hz, 8H, Ph-*H*), 7.33 (d, *J* = 7.5 Hz, 8H, Ph-*H*), 2.71 (t, *J* = 7.6 Hz, 8H, Alkyl-*H*), 1.75-1.66 (m, 8H, Alkyl-*H*), 1.44-1.31 (m, 24H, Alkyl-*H*), 0.91 (s, 12H, Me); ^{13}C NMR (100 MHz, $CDCl_3$): δ_C =141.98, 138.39, 137.11, 130.52, 129.58, 128.36, 128.01, 126.05, 125.21, 35.77, 31.79, 31.56, 29.10, 22.66, 14.16; FAB-MS: m/z calcd for $C_{64}H_{74}$ 843.5869 [M^+]; found 843.5840 [M^+].

X-ray Crystallography

A suitable single crystal of **TAPy** was obtained from dichloromethane/hexane or chloroform/methanol solutions, respectively. Single-crystal X-ray diffraction data was collected at 100(2) K on a XtaLAB Synergy-S, Dualflex, HyPix-6000HE diffractometer using Cu K radiation (λ = 1.5406 Å). The crystal was mounted on nylon CryoLoops with Paraton-N. The data collection and reduction were processed within *CrysAlisPro* (Rigaku OD, 2019). A multi-scan absorption correction was applied to the collected reflections. Using Olex^2, [50] the structure was solved with the ShelXT [51] structure solution program using Intrinsic Phasing and refined with the ShelXL [52] refinement package using Least Squares minimisation. All non-hydrogen atoms were refined anisotropically. The organic hydrogen atoms were generated geometrically. See Table S1 for crystal data. CCDC-2192451 contains supplementary crystallographic data for this paper. Copies of the data can be obtained, free of charge, on application to CCDC, 12 Union Road, Cambridge CB2 1EZ, UK [fax: 144-1223-336033 or e-mail: deposit@ccdc.cam.ac.uk].

Conflicts of interest

There are no conflicts to declare.

Acknowledgements

This work was performed under the Cooperative Research Program of “Network Joint Research Center for Materials and Devices (Institute for Materials Chemistry and Engineering, Kyushu University)”. We would like to thank the Natural Science Foundation of Shandong Province (Grant No. ZR2019BB067), this research used resources of the Advanced Light Source, which is a DOE Office of Science User Facility under contract no. DE-AC02-05CH11231. CR thanks the University of Hull for support.

References

[1] K.C. To, S. Ben-Jaber, I.P. Parkin, Recent Developments in the Field of Explosive Trace Detection, ACS Nano. 14 (2020) 10804–10833.

[2] S. Giannoukos, B. Brkić, S. Taylor, A. Marshall, G.F. Verbeck, Chemical Sniffing

Instrumentation for Security Applications, Chem. Rev. 116 (2016) 8146−8172.

[3] T.K. Naqvi, A.K. Srivastava, M.M. Kulkarni, A.M. Siddiqui, P.K. Dwivedi, Silver Nanoparticles Decorated Reduced Graphene Oxide (rGO) SERS Sensor for Multiple Analytes, Appl. Surf. Sci. 478 (2019) 887−895.

[4] Y. Gao, F. Chu, W. Chen, X. Wang, Y. Pan, Arc-Induced Nitrate Reagent Ion for Analysis of Trace Explosives on Surfaces Using Atmospheric Pressure Arc Desorption/Ionization Mass Spectrometry, Anal. Chem. 94 (2022) 5463–5468.

[5] E.V. Verbitskiy, G.L. Rusinov, O.N. Chupakhin, V.N. Charushin, Design of fluorescent sensors based on azaheterocyclic push-pull systems towards nitroaromatic explosives and related compounds: A review, Dyes Pigments. (180) 2020 108414.

[6] M.R. Eslami, N. Alizadeh, Ultrasensitive and Selective QCM Sensor for Detection of Trace Amounts of Nitroexplosive Vapors in Ambient Air Based on Polypyrrole-Bromophenol Blue Nanostructure, Sens. Actuators B Chemical. 278 (2019) 55−63.

[7] M.J. Kangas, R.M. Burks, J. Atwater, R.M. Lukowicz, P. Williams, A.E. Holmes, Colorimetric Sensor Arrays for the Detection and Identification of Chemical Weapons and Explosives, Crit. Rev. Anal. Chem. 47 (2017) 138−153.

[8] P.T. Charles, V. Wadhwa, A. Kouyate, K.J. Mesa-Donado, A.A. Adams, J.R. Deschamps, A.W. Kusterbeck, A High Aspect Ratio Bifurcated 128-Microchannel Microfluidic Device for Environmental Monitoring of Explosives, Sensors. 18 (2018) 1568.

[9] X. Sun, Y. Wang, Y. Lei, Fluorescence Based Explosive Detection: From Mechanisms to Sensory Materials, Chem. Soc. Rev. 44 (2015) 8019−8061.

[10] S.A.A. Razavi, A. Morsali, M. Piroozzadeh, A Dihydrotetrazine-Functionalized Metal–Organic Framework as a Highly Selective Luminescent Host–Guest Sensor for Detection of 2,4,6-Trinitrophenol, Inorg. Chem. 61 (2022) 7820–7834.

[11] P. Das, G. Chakraborty, S.K. Mandal, Comprehensive Structural and Microscopic Characterization of an Azine–Triazine-Functionalized Highly Crystalline Covalent Organic Framework and Its Selective Detection of Dichloran and 4-Nitroaniline, ACS Appl. Mater. Interfaces. 12 (2020) 10224–10232.

[12] G. Sathiyan, B. Balasubramaniam, S. Ranjan, S. Chatterjee, P. Sen, A. Garg, R.K.

Gupta, A. Singh, A novel star-shaped triazine-triphenylamineebased fluorescent chemosensor for the selective detection of picric acid, Mater. Today Chem. 12 (2019) 178–186.

[13] M.Z.K. Baig, P.K. Sahu, M. Sarkar, M. Chakravarty, Haloarene-Linked Unsymmetrically Substituted Triarylethenes: Small AIEgens To Detect Nitroaromatics and Volatile Organic Compounds, J. Org. Chem. 82 (2017) 13359–13367.

[14] S.H. Chen, K. Jiang, J.Y. Lin, K. Yang, X.Y. Cao, X.Y. Luo, Z.Y. Wang, Rational design and synthesis of Y-shaped fluorophores with multifarious emission properties and their application in the sensitive detection of PA, J. Mater. Chem. C. 8 (2020) 8257–8267.

[15] T. Wang, N. Zhang, R. Bai, Y. Bao, Aggregation-enhanced FRET-active conjugated polymer nanoparticles for picric acid sensing in aqueous solution, J. Mater. Chem. C. 6 (2018) 266–270.

[16] X. Guo, B. Gao, X. Cui, J. Wang, W. Dong, Q. Duan, T. Fei, Z. Su, PL sensor for sensitive and selective detection of 2,4,6-trinitrophenol based on carbazole and tetraphenylsilane polymer, Dyes Pigments 191 (2021) 109379.

[17] Z. Gou, X. Zhang, Y. Zuo, M. Tian, B. Dong, W. Lin, Pyrenyl-Functionalized Polysiloxane Based on Synergistic Effect for Highly Selective and Sensitive Detection of 4-Nitrotoluene, ACS Appl. Mater. Interfaces. 11 (2019) 30218–30227.

[18] D. Giri, S.K. Patra, 1, 2, 3-Triazolyl functionalized thiophene, carbazole and fluorene based A-alt-B type p-conjugated copolymers for the sensitive and selective detection of aqueous and vapor phase nitroaromatics (NACs), J. Mater. Chem. C. 8 (2020) 14469–14480.

[19] M.E. Germain, M.J. Knapp, Optical Explosives Detection: from Color Changes to Fluorescence Turn-on, Chem. Soc. Rev. 38 (2009) 2543−2555.

[20] M. Gao, B.Z. Tang, Fluorescent Sensors Based on Aggregation-Induced Emission: Recent Advances and Perspectives, ACS Sensors. 2 (2017) 1382−1399.

[21] T.M. Figueira-Duarte, K. Müllen, Chem. Rev. 111 (2011) 7260–7314.

[22] X. Feng, J.Y. Hu, C. Redshaw, T. Yamato, Functionalization of Pyrene To Prepare Luminescent Materials—Typical Examples of Synthetic Methodology, Chem. – Eur. J.

22 (2016) 11898–11916.

[23] H. Liu, J. Zeng, J. Guo, H. Nie, Z. Zhao, B.Z. Tang, High-Performance Non-doped OLEDs with Nearly 100 % Exciton Use and Negligible Efficiency Roll-Off, Angew. Chem. Int. Ed. 57 (2018) 9290.

[24] S. Gan, W. Luo, B. He, L. Chen, H. Nie, R. Hu, A. Qin, Z. Zhao, B.Z. Tang, Integration of aggregation-induced emission and delayed fluorescence into electronic donor–acceptor conjugates, J. Mater. Chem. C. 4 (2016) 3705.

[25] M.M. Islam, Z. Hu, Q.S. Wang, C. Redshaw, X. Feng, Pyrene-based aggregation-induced emission luminogens and their applications, Mater. Chem. Front. 3 (2019) 762–781.

[26] J. Mei, N.L.C. Leung, R.T.K. Kwok, J.W.Y. Lam, B.Z. Tang, Aggregation-Induced Emission: Together We Shine, United We Soar!, Chem. Rev. 115 (2015) 11718−11940.

[27] H. Zhang, Z. Zhao, A.T. Turley, L. Wang, P.R. McGonigal, Y. Tu, Y.Y. Li, Z. Wang, R.T.K. Kwok, J.W.Y. Lam, B.Z. Tang, Aggregate Science: From Structures to Properties, Adv. Mater. 32 (2020) 2001457.

[28] K.H. Lee, J.K. Park, J.H. Seo, S.W. Park, Y.S. Kim, Y.K. Kim, S.S. Yoon, Efficient deep-blue and white organic light-emitting diodes based on triphenylsilane-substituted anthracene derivatives, J. Mater. Chem. 21 (2011) 13640−13648.

[29] X. Feng, H. Tomiyasu, J.Y. Hu, X. Wei, C. Redshaw, M.R.J. Elsegood, L. Horsburgh, S.J. Teat, T. Yamato, J. Org. Chem. 80 (2015) 10973−10978.

[30] Z.D. Yu, X.X. Dong, J.Y. Cao, W.X. Zhao, G.H. Bi, C.Z. Wang, T. Zhang, S. Rahman, P.E. Georghiou, J.B. Lin, T. Yamato, Substituent effects on the intermolecular interactions and emission behaviors in pyrene-based mechanochromic luminogens, J. Mater. Chem. C. 10 (2022) 9310–9318.

[31] R.W. Newberry, R.T. Raines, A prevalent intraresidue hydrogen bond stabilizes proteins, Nat. Chem. Biol. 12 (2016) 1084–1088.

[32] R.D. Crocker, D.P. Pace, B.L. Zhang, D.J.M. Lyons, M.M. Bhadbhade, W.W.H. Wong, B.K. Mai, T.V. Nguyen, Unusual Alternating Crystallization-Induced Emission Enhancement Behavior in Nonconjugated ω-Phenylalkyl Tropylium Salts, J. Am. Chem. Soc. 143 (2021) 20384–20394.

[33] H. Zhang, F. Tao, Z. Xu, Y. Cui, W.W. Yu, D. Zhang, Data encryption-decryption based on crystal-induced emission enhancement (CIEE) properties of barbituric acid derivatives, Dyes Pigments. 180 (2020) 108408.

[34] C.Z. Wang, Z.J. Pang, Z.D. Yu, Z.X. Zeng, W.X. Zhao, Z.Y. Zhou, C. Redshaw, T. Yamato, Tetrahedron. 78 (2021) 131828.

[35] Z.D. Yu, J.Y. Cao, H.L. Li, G. Yang, Z.M. Xue, L. Jiang, J.Y. Yu, C.Z. Wang, X.Y. Liu, C. Redshawd, T. Yamato, Structure-controlled intramolecular charge transfer in asymmetric pyrene-based luminogens: Synthesis, characterization and optical properties, New J. Chem. 2022,

[36] S. Grimme, J. Antony, S. Ehrlich, H. Krieg, A consistent and accurate ab initio parametrization of density functional dispersion correction (DFT-D) for the 94 elements H-Pu, J. Chem. Phys. 132 (2010) 154104.

[37] J. Liu, Y. Zhang, K. Zhang, J. Fan, C.K. Wang, L. Lin, Bicolor switching mechanism of multifunctional light-emitting molecular material in solid phase, Org. Electron. 71 (2019) 212–219.

[38] L.J. Tu, W.L. Che, S.H. Li, X.N. Li, Y. Xie, Z. Li, Alkyl chain regulation: distinctive odd–even effects of mechano-luminescence and room-temperature phosphorescence in alkyl substituted carbazole amide derivatives, J. Mater. Chem. C. 9 (2021) 12124–12132.

[39] H. Liu, Y. Dai, Y. Gao, H. Gao, L. Yao, S. Zhang, Z. Xie, K. Wang, B. Zou, B. Yang, Y. Ma, Monodisperse π-π stacking anthracene dimer under pressure: Unique fluorescence behaviors and experimental determination of interplanar distance at excimer equilibrium geometry, Adv. Opt. Mater. 6 (2018) 1800085.

[40] H. Liu, Y. Gu, Y. Dai, K. Wang, S. Zhang, G. Chen, B. Zou, B. Yang, Pressure-Induced Blue-Shifted and Enhanced Emission: A Cooperative Effect between Aggregation-Induced Emission and Energy-Transfer Suppression, J. Am. Chem. Soc. 142 (2020) 1153−1158.

[41] X. Wang, J. Zhang, X. Mao, Y. Liu, R. Li, J. Bai, J. Zhang, C. Redshaw, X. Feng, B.Z. Tang, Intermolecular Hydrogen-Bond-Assisted Solid-State Dual-Emission Molecules with Mechanical Force-Induced Enhanced Emission, J. Org. Chem. 87

(2022) 8503–8514.

[42] X. Luo, J. Li, C. Li, L. Heng, Y. Dong, Z. Liu, Z. Bo, B.Z. Tang, Reversible Switching of the Emission of Diphenyldibenzofulvenes by Thermal and Mechanical Stimuli, Adv. Mater. 23 (2011) 3261–3265.

[43] C.Z. Wang, X. Feng, Z. Kowser, C. Wu, T. Akther, M.R.J. Elsegood, C. Redshaw T. Yamato, Pyrene-based color-tunable dipolar molecules: Synthesis, characterization and optical properties, Dyes Pigments. 153 (2018) 125–131.

[44] C.Z. Wang, H. Ichiyanagi, K. Sakaguchi, X. Feng, M.R.J. Elsegood, C. Redshaw T. Yamato, Pyrene-Based Approach to Tune Emission Color from Blue to Yellow, J. Org. Chem. 82 (2017) 7176–7182.

[45] X. Feng, Z. Xu, Z. Hu, C. Qi, D.X. Luo, X. Zhao, Z. Mu, C. Redshaw, J.W.Y. Lam, D. Ma, B.Z. Tang, Pyrene-based blue emitters with aggregation-induced emission features for high-performance organic light-emitting diodes, J. Mater. Chem. C. 7 (2019) 2283−2290.

[46] N.N. Ji, Z.Q. Shi, H.L. Hu, H.G. Zheng, A triphenylamine-functionalized luminescent sensor for efficient p-nitroaniline detection, Dalton Trans. 47 (2018) 7222–7228.

[47] B. Gole, W. Song, M. Lackinger, P.S. Mukherjee, Explosives Sensing by Using Electron-Rich Supramolecular Polymers: Role of Intermolecular Hydrogen Bonding in Significant Enhancement of Sensitivity, Chem. – Eur. J. 20 (2014) 13662 – 13680.

[48] A. Kathiravan, A. Gowri, T. Khamrang, M.D. Kumar, N. Dhenadhayalan, K.C. Lin, M. Velusamy, M. Jaccob, Pyrene-Based Chemosensor for Picric Acid–Fundamentals to Smartphone Device Design, Anal. Chem. 91(2019) 13244−13250.

[49] S.Y. Kim, M.J. Kim, M. Ahn, K.M. Lee, K.R. Wee, Systematic energy band gap control of pyrene-based donor-acceptor-donor molecules for efficient chemosensor, Dyes Pigments. 191 (2021) 109362.

[50] O.V. Dolomanov, L.J. Bourhis, R.J. Gildea, J.A.K. Howard, H. Puschmann, J. Appl. Crystallogr. 42 (2009) 339–341.

[51] G.M. Sheldrick, Acta Crystallogr., Sect. A: Found. Adv. A71 (2015) 3–8.

[52] G.M. Sheldrick, Acta Crystallogr., Sect. C: Struct. Chem. C71 (2015) 3–8.